


Article

Mammalian Cell Cytotoxicity, Antibacterial Activity and the Properties of Methylenebis(Hydroxybenzoic Acid) and Its Related Zinc(II) Complex

Ayman H. Ahmed ^{1,*} , Ibrahim O. Althobaiti ¹, Marwah Aljohani ², Ehab S. Gad ¹, Yazeed M. Asiri ³ and Omar A. Hussein ⁴

¹ Department of Chemistry, College of Science and Arts, Jouf University, Gurayat 2014, Saudi Arabia; ioalthobaiti@ju.edu.sa (I.O.A.); esgad@ju.edu.sa (E.S.G.)

² Department of Chemistry, College of Science, Imam Abdulrahman Bin Faisal University, P.O. Box 76971, Dammam 31441, Saudi Arabia; mhaljohani@iau.edu.sa

³ Department of Chemistry, College of Science, Taif University, P.O. Box 11099, Taif 21944, Saudi Arabia; y.asiree@tu.edu.sa

⁴ Faculty of Medicine, Benha University, Benha 13518, Egypt; omar406876@fmed.bu.edu.eg

* Correspondence: ahfahmi@ju.edu.sa

Abstract: Formaldehyde, sulfuric acid and salicylic acid were combined to create a 3,3'-methylenebis(2-hydroxybenzoic acid) (MHB) ligand, which was subsequently permitted to bind with zinc(II) ions. The ligand and its zinc(II) complex (Zn–MHB) have been described by a combination of elemental analyses, spectral analyses (UV–Vis, IR, MS and NMR), XRD, TEM, as well as TGA measurement. The ligand has been suggested to coordinate to the zinc center in a tetradentate manner forming the binuclear tetrahedral complex. An X-ray analysis indicated a considerable difference between MHB (crystalline) and Zn–MHB (amorphous). The UV–Vis spectra were used to determine the optical properties such as bandgap, refractive index, optical conductivity and penetration depth. The possibility of employing the samples for optoelectronic applications was indicated from the band gap values which underlie the range of semiconductors. TEM revealed the spherical shapes and mutation of ligand particles into the nano-scale by complexation. The antimicrobial potential of the MHB towards Gram-positive and Gram-negative bacterial growths has been investigated. The results suggested that it would be possible to employ MHB to prevent bacterial development, particularly that of salmonella typhimurium. The cytotoxicity of the MHB was assessed against two types of mammalian cells: VERO (the kidney of an African green monkey) and HFB4 (human skin melanocytes). Lower sensitivity was observed in VERO cells.

Keywords: methylenebis(hydroxybenzoic acid); zinc complex; spectral characterization; optical properties; biological evaluation



Citation: Ahmed, A.H.; Althobaiti, I.O.; Aljohani, M.; Gad, E.S.; Asiri, Y.M.; Hussein, O.A. Mammalian Cell Cytotoxicity, Antibacterial Activity and the Properties of Methylenebis(Hydroxybenzoic Acid) and Its Related Zinc(II) Complex. *Crystals* **2024**, *14*, 88. <https://doi.org/10.3390/cryst14010088>

Academic Editors: Simona Nica and Pedro Netto Batalha

Received: 24 December 2023

Revised: 11 January 2024

Accepted: 13 January 2024

Published: 17 January 2024



Copyright: © 2024 by the authors. Licensee MDPI, Basel, Switzerland. This article is an open access article distributed under the terms and conditions of the Creative Commons Attribution (CC BY) license (<https://creativecommons.org/licenses/by/4.0/>).

1. Introduction

Methylenebis(hydroxybenzoic acid) has acquired prominence because it serves as a polyfunctional intermediate in condensation products that are appropriate for the surface coatings and plastics industries. Literature has documented just a few syntheses of certain methylenebis(hydroxybenzoic acid) compounds [1]. Recently, the very selective extractions of Pb(II) over Ni(II), Cd(II), Cu(II) and Zn(II) from aqueous solution into chloroform was studied for methylenebis(hydroxybenzoic acid) ligands having different spacers between two hydroxybenzoic/salicylic acid units [2]. It was reported that an ethylene spacer shows a superior Pb(II) extraction selectivity compared to Cu(II). It is evident from the literature that efforts were made to create solid 3,3'-methylenebis(2-hydroxybenzoic acid) (MHB) complexes by traditional techniques. However, not much physico-chemical research has been performed on MHB complexes. The MHB is capable of producing chelated

colorful compounds when combined with copper and iron; in addition, Ba and Mg-MHB were prepared [3]. It is noteworthy that 5, 5'-methylenedisalicylic acid, which is highly similar to MHB, may establish a solid complex with aluminum and rare earths (M = La, Ce, Pr, Nd, Sm, Gd, Ho, Yb, or Y) [4]. The physicochemical research on square planar Cu^{II} , Ni^{II} and Co^{II} complexes with bis-oxime of 5,5'-methylene(salicylaldehyde) has been discussed by Patel et al. [5]. The results indicated that the thermal stability of the complexes displays the following arrangement: $\text{Co}(\text{II}) > \text{Ni}(\text{II}) > \text{Cu}(\text{II})$. Some enzymes or catalysts in biological reactions are built from zinc complexes [6,7]. Transition metal–polycarboxylate complexes have fascinating magnetic, biological and structural characteristics [8–11]. The applications of the transition metal complexes of methylenebis(hydroxybenzoic acid) in catalysis, bioinorganic, electrochemistry, corrosion, metallic deactivators, environmental chemistry and separation methods are noteworthy [5,12–14].

Bacterial resistance is a significant issue for public health. The World Health Organization, or WHO, has reported that bacterial natural phenomena can cause fundamental antibiotics to lose their efficacy in multiple cases [15]. The fact that many pathogenic bacteria have developed resistance makes research into novel antimicrobial drugs crucial. Chemotherapeutic agents are the names given to the chemical substances that have been created and are used to treat infectious diseases. Thousands of compounds are created annually to discover potential chemotherapeutic agents to combat harmful microbes. Since salicylic acid, which possesses antibacterial and antiseptic effects, has a structure that is quite similar to MHB, the MHB was chosen to examine its bacterial effect. Salicylic acid and some of its derivatives, which have structures resembling MHB, and contain OH and COOH groups, have been described in the literature and reveal antibacterial effects [16–19].

The purpose of this work is to synthesize and characterize 3,3'-methylenebis(hydroxybenzoic acid), (MHB) and its Zn(II) complex. Several techniques have been used to describe the isolated materials. The optical parameters like penetration depth, optical conductivity, band gap and refractive index were also determined. The investigation also aimed to explore the biological impacts of the ligand (MHB) on the bacteria and normal mammalian cells in order to provide insights into potential therapeutic applications.

2. Experimental

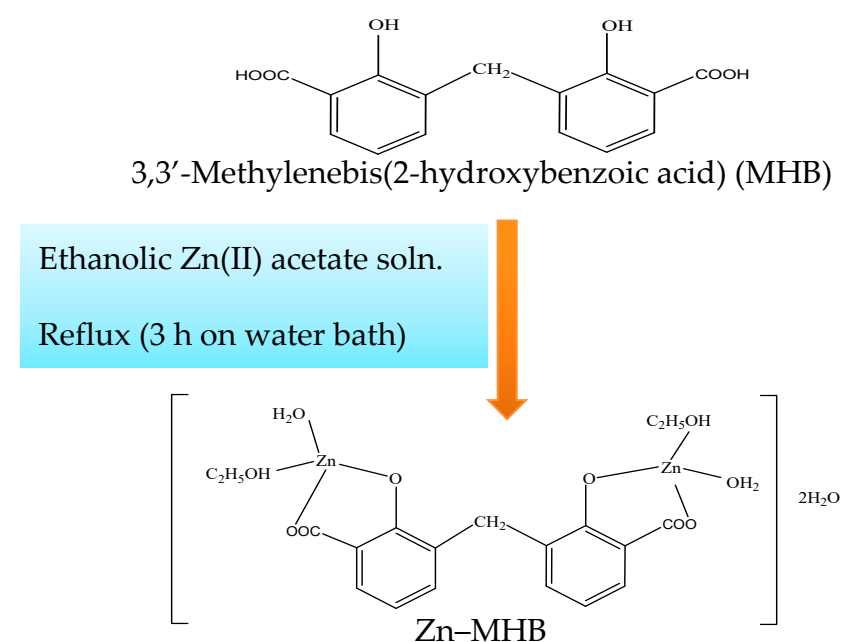
2.1. Materials and Methods

The highest grade reagents from BDH, London, UK, were all used without further purification. Trypan blue dye and MTT were obtained from Sigma, St. Louis, MO, USA. DMEM, fetal bovine serum, HEPES buffer solution, gentamycin, L-glutamine and 0.25% trypsin-EDTA were bought from Lonza, Verviers, Belgium. ATCC (The American Type Culture Collection) provided the mammalian cells: VERO (African Green Monkey kidney) and HFB4 (human normal melanocytes of skin). The elemental analysis (C, H), metal content (wt%) and melting point were estimated as previously indicated [20]. The IR spectra were recorded using the ATR method using Thermo Scientific's iS50 FT-IR spectrometer. At room temperature, a Bruker spectrometer was used to perform an $^1\text{H-NMR}$ (400 MHz) analysis in dimethylsulfoxide. With the help of tetramethylsilane, (TMS) as an internal reference, the chemical changes are stated in parts per million (ppm). The thermo scientific GCMS model ISQ at the Regional Center for Mycology and Biotechnology (RCMB), Al-Azhar University (Cairo, Egypt), was used for mass spectroscopy. The direct Inlet component of the mass analyzer was used for this purpose. The mass spectroscopy technique was utilized to determine the molecular weight expectation of the compound. The electron impact mode was used for the mass spectrometry. Using a Perkin-Elmer lambda 35 UV-Vis Spectrophotometer and the Nujol-mull approach, electronic spectra were captured in the range of 200–1100 nm. With a Shimadzu 50 H thermal analyzer, thermal analysis (TG) was conducted under nitrogen. A drop of the solution was put to the carbon-coated copper grids for TEM analysis, and the drop was allowed to dry at room temperature. The Regional Center for Mycology and Biotechnology (RCMB) in Egypt used a JEOL GEM-1010 transmission electron microscope operating at 80 kV to collect the

electron micrographs. Germany's XRD Bruker Co. D₈ Discover was used to examine the crystallinity of MHB and the Zn(II) complex over 2 angles ranging from 3 to 80 degrees with Cu target K radiation (1.54 Å, 40 kV and 40 mA). The band gap energy (E_g) of MHB and its corresponding Zn(II) complex were computed in order to elucidate the conductivity of the separated compounds [21–23]. The approximate absorption coefficient (α) was determined by applying the formula $\alpha = 1/d \ln(1/T)$, where T is the measured transmittance and d is the cell width. With the use of the Tuac equation, $\alpha h\nu = A(h\nu - E_g)^m$, and the optical band gap was calculated. A is an energy-independent constant, and m is equal to 1/2 and 2 for direct and indirect transitions, respectively. From the plot of $(\alpha h\nu)^2$ vs. $h\nu$, an indirect band gap was determined by extending the linear part of the curve to $(\alpha h\nu)^2 = 0$. Antibacterial and cytotoxicity evaluations were conducted at RCMB, Egypt.

2.2. Sample Collection (MHB and Zn–MHB)

3,3'-Methylenebis(2-hydroxybenzoic acid), MHB, Scheme 1, was obtained using the recipe outlined in the literature [2–4] as follows: 180 g of 50% sulfuric acid, 27.6 g of hydroxybenzoic acid and 9.4 g of 30% formaldehyde, which were refluxed for 7 h. To remove any remaining unreacted hydroxybenzoic acid, the separated powder was allowed to cool, filtered out, extensively cleaned with cold water and then hot water/ethanol solutions. After being separated and recrystallized from acetone, the cream powder was allowed to air dry for 48 h. The MHB is soluble in ethanol, acetone, carbon tetrachloride, diethyl ether, dimethylformamide (DMF) and dimethylsulphoxide (DMSO) but insoluble in water. Cream powder, yield 96%, m.p. 238 °C. Found (%): C, 62.10; H, 4.01. C₁₅H₁₂O₆. Calculated (%): C, 62.50; H, 4.20.



Scheme 1. Schematic diagram of Zn–MHB complex formation.

By mixing ethanolic solutions of 0.01 mol MHB with 0.02 mol Zn(II) acetate, the Zn–MHB complex was created. In a water bath, the reaction mixtures were refluxed for three hours. The colored granules were heated, filtered and thoroughly washed with hot ethanol before being dried in the air. The fact that the complex is insoluble in typical organic solvents indicates that the function of the polar groups (OH, COOH) has been lost. This can be interpreted as proof that the deprotonated hydroxyl and carboxyl groups of the ligand successfully coordinated with the metal. White powder, yield 85%, m.p. > 300 °C. Found (%): C, 39.40; H, 4.86; M, 22.50. C₁₉H₂₈O₁₂Zn₂. Calculated (%): C, 39.40; H, 4.87; M, 22.58.

2.3. Pharmacological Screening of MHB

2.3.1. Antibacterial Activity

NCCLS (1993; National Committee for Clinical Laboratory Standards) guidelines were followed for conducting the susceptibility tests. We used the well diffusion approach to conduct screening tests related to the inhibition zone [24]. The inoculum suspension was obtained by inoculating Mueller–Hinton broth (fungi utilizing malt broth) with colonies grown overnight on a plate of agar. The MHB compound was dissolved in DMSO at three different doses: 2.5, 5 and 10 mg/mL. To inoculate Mueller–Hinton agar plates, a sterile swab had been dipped in the suspension. An inhibition zone was determined surrounding each well after a 24 h period at 37 °C. The correct execution of the DMSO controls was made.

2.3.2. Cytotoxic Assessment

The cells were grown in a medium called Dulbecco's modified Eagle's, which was enriched with 50 µg/mL of gentamycin, 10% heat-inactivated fetal bovine serum, 1% L-glutamine and HEPES buffer. Every cell was cultivated twice a week at 37 °C in a humidified environment with 5% CO₂.

The cytotoxicity experiment [25,26] was conducted using a viability assay in which 100 µL of growth medium was added to 96-well plates at a cell concentration of 1×10^4 per well. After 24 h of seeding, fresh medium with varying quantities of the test sample was introduced. Confluent cell monolayers were pipetted into 96-well flat-bottomed micro-titer plates (Falcon, NJ, USA) using a multichannel pipette, and serial two-fold dilutions of the chemical component under test were added. For twenty-four hours, the micro-titer plates were kept at 37 °C in a humidified incubator with 5% CO₂. For every test sample concentration, three wells were utilized. Control cells have been incubated with or without DMSO and without the test sample. There was no impact of the small amount of DMSO (maximum 0.1%) on the experiment. The MTT test was used in a colorimetric technique to measure the viable cell yield following the incubation of the cells. The 96-well plate's medium was taken out and 100 µL of fresh culture RPMI 1640 medium without phenol red was added instead. Thereafter, 10 µL of the 12 mM MTT stock solution—which contains 5 mg of MTT in 1 mL of PBS—was added to every well, including the untreated controls. After that, the 96-well plates were incubated for four hours at 37 °C with 5% CO₂. After removing an 85 µL aliquot of the medium from each well, 50 µL of DMSO was added, thoroughly mixed, and the wells were incubated for 10 min at 37 °C. The number of live cells was next ascertained by measuring the optical density at 590 nm using a micro plate reader (Sun Rise, TECAN, Inc., Redwood City, CA 94063, USA). $[(\text{ODt}/\text{ODc})] \times 100\%$ was the formula used to obtain the viability percentage; ODt denotes the mean optical density of the wells treated with the tested sample, and ODc denotes the mean optical density of the cells that were left untreated. The survival curve of each tumor cell line following treatment with the designated substance is obtained by plotting the relationship between the remaining cells and compound concentration. Using graphic plots of the dose–response curve for each concentration, the cytotoxic concentration (CC₅₀), or the concentration needed to cause toxic effects in 50% of intact cells, was determined using the Graphpad Prism software, version 10.0.0 for Windows (San Diego, CA, USA).

3. Results and Discussion

Various physicochemical methods were used to validate the structural formula of the produced molecules.

3.1. Sample Characterization

3.1.1. Structural Determination of the Ligand, MHB

Mass spectrum: The predicted molecular weight of the compound was emphasized throughout the mass spectrum (Figure 1). The molecular ion peak for the MHB was at $m/e = 288.35$ ((C₁₅H₁₂O₆), calculated $m/e = 288.35$).

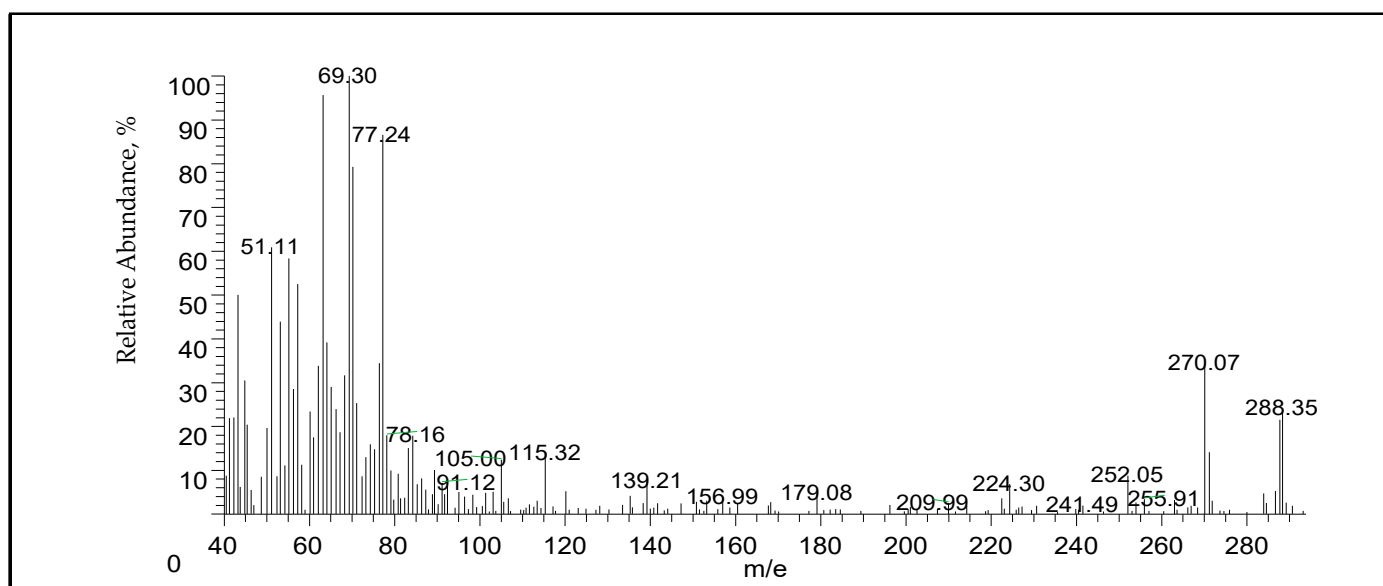


Figure 1. Mass spectrum of MHB.

IR spectrum: The spectrum data (Figure 2, Table 1) exhibited $\nu(\text{C-O})_{\text{phenolic}}$, $\nu(\text{OH})_{\text{phenolic}}$, $\delta(\text{OH})_{\text{phenolic}}$ and $\nu(\text{C=O})_{\text{caroxylic}}$ at 1281, 3150, 1200 and 1648 cm^{-1} , respectively [27]. It is believed that the presence of the phenolic OH at the lower site (3150 cm^{-1}) indicates that intermolecular H-bonding (O–H...O–H) between related molecules. The widening shape of $\nu\text{OH}_{\text{phenolic}}$ provides support for this suggestion, whereas the band resulting from intramolecular hydrogen bonds is sharp. The significant reduction in frequency reveals how strong the link is. The broad band at 2395–2650 cm^{-1} confirms the presence of the intermolecular hydrogen bond among MHB molecules.

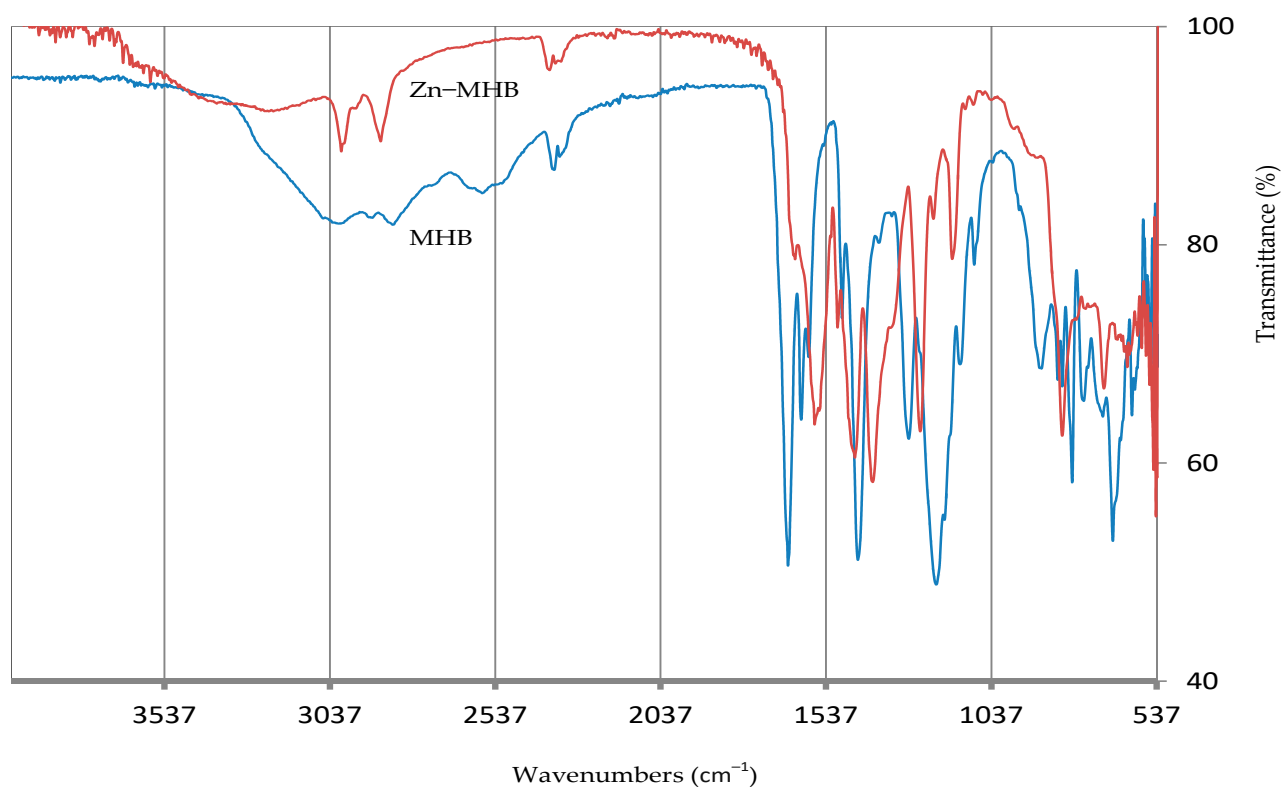


Figure 2. FT-IR spectra of MHB ligand and Zn–MHB complex.

Table 1. Significant IR and XRD data of the zinc(II) complex and free ligand.

Compound	Wavenumbers of Infrared Data (cm ⁻¹)						XRD Data			
	Phenolic (OH) Str.	Phenolic (OH) Bend.	Phenolic (C–O) Str.	Carboxylic (OH) (H-Bond) Str.	(C=O) L: Carboxylic Complex: Carboxylate Str.	(Zn–O) Str.	Angle (d Value)	θ°	β (Rad)	D (nm)
MHB	≈3150	1200	1281	2395–3650	1648	-	13.206° (6.699 Å), 15.324° (5.777 Å), 16.239° (5.454 Å), 19.169° (4.626 Å), 19.797° (4.481 Å), 22.694° (3.915 Å), 23.424° (3.795 Å), 26.521° (3.358 Å), 29.789° (2.997 Å), 30.990° (2.883 Å), 34.075° (2.629 Å), 35.858° (2.502 Å), 38.488° (2.337 Å), 40.300° (2.236 Å), 42.072° (2.146 Å)	23.47	0.0105	15.1
Zn-MHB	-	-	1248	-	1554	618, 624	7.387° (11.95800 Å)	-	-	-

The absorption of the $(\text{C}=\text{O})_{\text{carboxyl}}$ is lower than the typical position ($1700\text{--}1730\text{ cm}^{-1}$) due to the presence of MHB as a dimer (intermolecular hydrogen bonding) and internal conjugation (the lone pair on the carboxyl's OH is in delocalization with $\text{C}=\text{O}$). Four bands associated with aromatic ($\text{C}=\text{C}$) vibrations were also found at 1609 , 1585 , 1489 and 1435 cm^{-1} . Moreover, Figure 2 shows the locations of additional bands corresponding to the phenyl rings at 791 cm^{-1} (out-of-plane deformation), $\nu\text{CH}_{\text{aromatic}}$ (near 3033 cm^{-1}) and methylene ($-\text{CH}_2-$) groups ($\nu\text{CH}_{\text{asym}} = 2905$, $\nu\text{CH}_{\text{sym}} = 2836$ and $\delta\text{CH}_{\text{rocking}} = 754\text{ cm}^{-1}$).

NMR spectrum: According to a prior report [2], the ^1H NMR spectrum of the MHB revealed signals at 2.5 (CH_2 , d), 11.2 (COOH , s, broad), 11.6 (phenolic OH, s, broad) and $6.7\text{--}7.9$ (aromatic protons, m), Figure 3. The correct locations of $-\text{OH}$ groups and $-\text{COOH}$, where the labile protons can be replaced by deuterium, were demonstrated by the disappearing signals of $-\text{COOH}$ and $-\text{OH}$ following the addition of D_2O . In accordance with the infrared data, the broadening of the $\text{OH}_{\text{phenolic}}$ and COOH signals in the spectrum provided evidence for the existence of intermolecular hydrogen bonding for these groups.

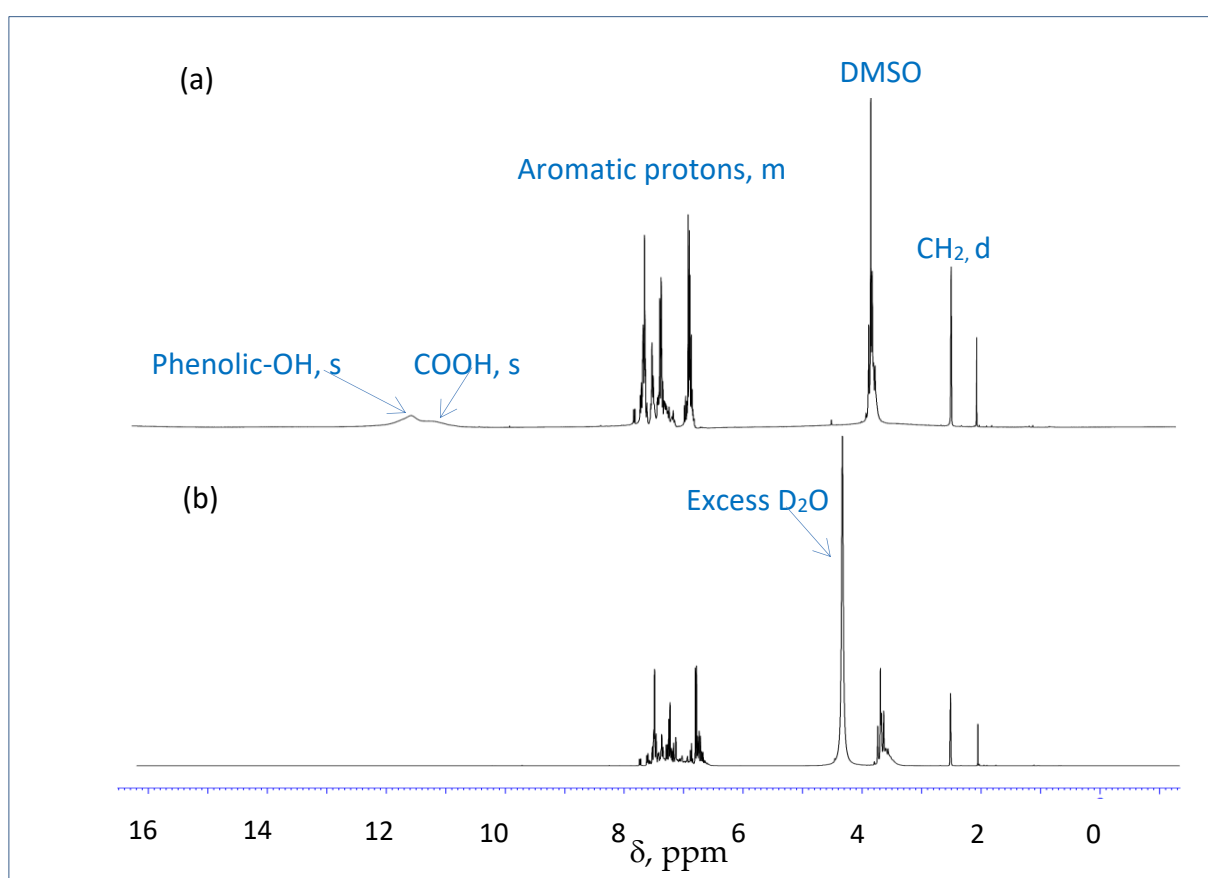


Figure 3. ^1H NMR spectrum of the MHB in (a) $\text{DMSO } d_6$ and (b) $\text{DMSO } d_6 + \text{D}_2\text{O}$.

3.1.2. Structural Determination of the Complex, Zn-MHB

Along with their diamagnetism and white color, the Zn^{II} (d^{10} configuration) could be regarded as a limit for the spectroscopic description of Zn derivatives due to their diamagnetism and white color. Conversely, the lack of ligand field stabilization might provide extremely flexible coordination geometry that is exclusively controlled by the ligands' charge and steric hindrance [28,29].

IR spectrum: A comparison between the IR spectrum of the complex and that of MHB (Figure 2, Table 1) signified that MHB acts as a tetradentate ligand chelating two zinc ions via the deprotonated phenolic ($-\text{OH}$) and carboxyl (COOH) groups. The following evidence supports this suggestion: (1) The negative shift of the $\nu(\text{C}-\text{O})$ band (MHB: $1281 \rightarrow \text{Zn-MHB}$:

1248 cm^{-1}). (2) The disappearance of ν and $\delta(\text{OH})_{\text{phenolic}}$ in the ligand upon complexation. (3) The carbonyl group ($\text{C}=\text{O}$) of the carboxyl (L : 1648 cm^{-1} , Table 1) disappears and the carbonyl of the carboxylate appears instead at 1554 cm^{-1} . (4) The obscure broad band assigned to the intermolecular H-bond of COOH in the ligand (2395–2650 cm^{-1}) points to the breakage of this bond by the coordination with zinc. The persistence of two additional bands in the range of 600–620 cm^{-1} , centered at 618 and 624 due to $(\text{Zn}-\text{O})$ [30], is further evidence of the coordination of phenolic and carboxylic oxygen. On the other hand, the coordinated ethanol and water in the complex are indicated by the stretching vibrations observed within 3450–3550 cm^{-1} ($\nu\text{OH}_{\text{ethanol}}$, $\nu\text{OH}_{\text{water}}$) and two somewhat weaker bands assigned to rocking (OH_{water} , 870 cm^{-1}) and wagging (OH_{water} , 614 cm^{-1}) vibrations.

UV-Vis spectrum: The electronic spectrum of the MHB and Zn-MHB were scanned and shown in Figure 4. MHB gave five peaks centered at 361, 351, 341, 319 and 280 associated with $n \rightarrow \pi^*$ ($\text{C}=\text{O}_{\text{carboxyl}}$), $n \rightarrow \pi^*$ phenolic OH, $\pi \rightarrow \pi^*$ ($\text{C}=\text{O}$), $\pi \rightarrow \pi^*$ phenolic and $\pi \rightarrow \pi^*$ (phenyl) transitions, respectively. The $\pi \rightarrow \pi^*$ and $n \rightarrow \pi^*$ transitions were suggested for phenolic OH considering it is in delocalization with the $\text{C}=\text{O}$ of the carboxyl group. As it is well known, the $\text{Zn}(\text{II})$ complexes do not display d-d transitions due to their fully filled d^{10} configuration; however, they frequently show the charge transfer spectra. The same MHB peak locations with a slight shift were visible in the Zn-MHB electronic spectrum, along with the peak of absorption at 420 nm due to L-M charge transfer (LMCT). The existence of the latter new CT band is consistent with the complex having a tetrahedral structure [31] and confirmed the coordination of MHB with the $\text{Zn}(\text{II})$ ion.

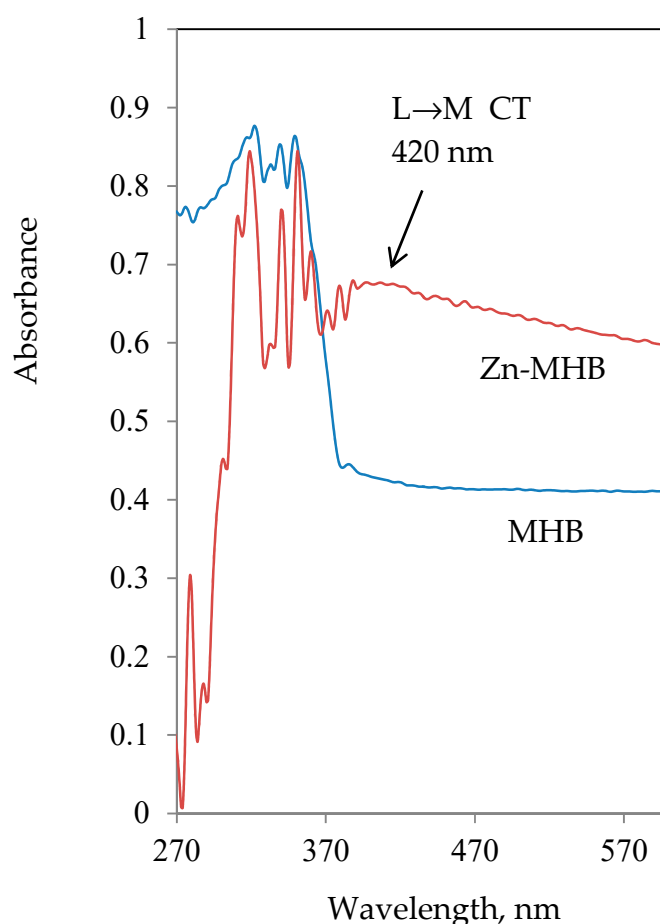


Figure 4. Electronic spectrum of MHB and Zn-MHB.

Thermogravimetric analysis: The thermogram of the Zn-MHB has been studied. The TG curves up to 800 $^{\circ}\text{C}$ (Figure 5) revealed several weight loss steps. The first one (40–110 $^{\circ}\text{C}$) is caused by the elimination of crystalline water molecules (found/calculated

= 6.6/6.2%); the second weight loss stage (110–280 °C) arises from the removal of the two coordinated water molecules (found/calculated = 6.7/6.2%); whereas the third weight loss step (280–400 °C) comes from the elimination of coordinated ethanol (found/calculated = 14.4/15.9)%. The other four peaks are the result of the Zn(II) complex decomposition, which produces metal oxides in the last stage.

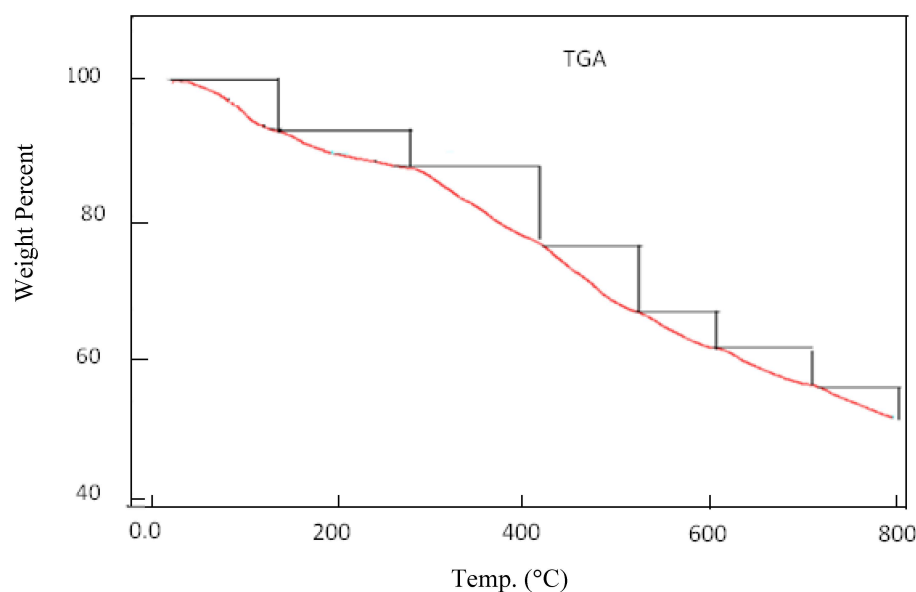


Figure 5. TGA of Zn-MHB.

In light of the results mentioned above, the logical structure of the Zn(II) chelate is displayed in Scheme 1. A tetrahedral confirmation for Zn-MHB is supported by the fact that Zn(II) ion is a late transition metal with full d valence electrons, meaning that a stable 18-electron complex may be produced through a four-coordination number.

3.1.3. Powder XRD Studies

X-ray diffraction patterns are recorded for MHB and Zn(II) complex. The patterns of the samples are presented in Figure 6 and the diffraction data include the inter-planar distances d (Å) and the crystallite size are given in Table 1. The findings show that the MHB is crystalline, i.e., it contains a definite arrangement of particles. The very good crystallinity of the MHB particles is really indicated by well-defined sharp peaks in the XRD patterns [32]. The XRD pattern of Zn-MHB indicated an amorphous character, suggesting that the constituent particles are randomly arranged. In X-ray diffraction and crystallography, the Scherrer equation [33] is a formula used to estimate the smallest size or diameter of a nanogranule; it is not relevant in limits larger than 200 nm. The Debye-Scherrer equation is

$$D = k\lambda / \beta \cos \theta;$$

where λ = wavelength of X-ray radiation (Cu $K\alpha$ = 1.54 Å); β = the line broadening at full width at half-maximum height (FWHM) in radians; k = constant taken as 0.94; θ = diffraction angle in degree; and D = average crystallite size (Å). The MHB crystallite size was found to be 15.1 nm. The amorphous nature of Zn-MHB precluded the application of the Debye-Scherrer equation.

3.1.4. Optical Properties

The transmittance spectrum measurements were used to study the optical characteristics of the compounds. Figure 7a shows the transmittance that was obtained. The energy gap (E_g) is the amount of energy required to move an electron from the valence band to the conduction band. Both the resultant electron in the conduction band and the electron

hole in the valence band are free to migrate inside the crystal lattice and carry out electrical current conductivity. Small band gaps (from 0.1 to <4 electron volts, eV) are found in semiconductors, big-band gaps (>4 eV) are found in insulators and conductors have very small band gaps or none at all because the valence and conduction bands overlap to produce a continuous band. Since the band gap value determines the material's optical characteristics, or its capacity to absorb light or photon energy, it was necessary to measure it. The values of the indirect optical band gap were computed and are displayed in Figure 7b. The MHB and Zn-MHB were discovered to have E_g values of 3.23 and 3.16 eV, respectively. The result indicates that the conduction of the ligand and the complex resemble ZnO ($E_g = 3.37$), GaN ($E_g = 3.4$) and ZnSe ($E_g = 2.7$) [34]. As reported in the literature [35], it could be explained that the slightly higher E_g values of MHB in comparison to its analogous Zn(II) complex. Through the acceptance of ligand electrons in its shell, zinc tends to increase the ligand mobilization. It can be found that, after chelation, the localized levels' width is increased, resulting in a reduced band gap. It is noteworthy to emphasize that a small band gap facilitates electronic transitions between the HOMO-LUMO energy states, increasing the molecule's electro-conductivity [36]. The MHB and Zn(II) complexes both have band gap values lying in the range of semiconductors and could be employed in the applications of optoelectronic [37].

The refractive index, which controls the speed of light in media other than a vacuum, is an essential property for optical applications. The smaller the refractive index (n), the higher the light travels through the substance. The evaluation of optical materials' refractive indices is crucial for their application in optic devices, such as switches and modulators. Furthermore, one important physical characteristic that is commonly used in chemistry to assess purity is the refractive index. The subsequent relationship has been used to estimate the reflectance:

$$R + T + A = 1$$

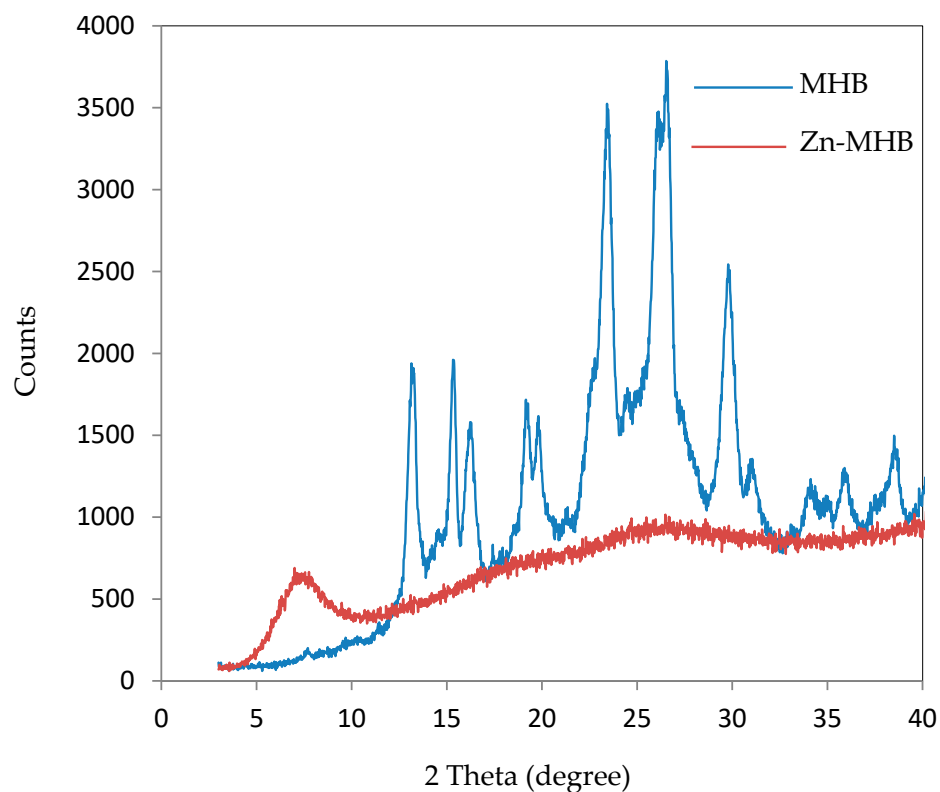


Figure 6. XRD graph of MHB and Zn-MHB.

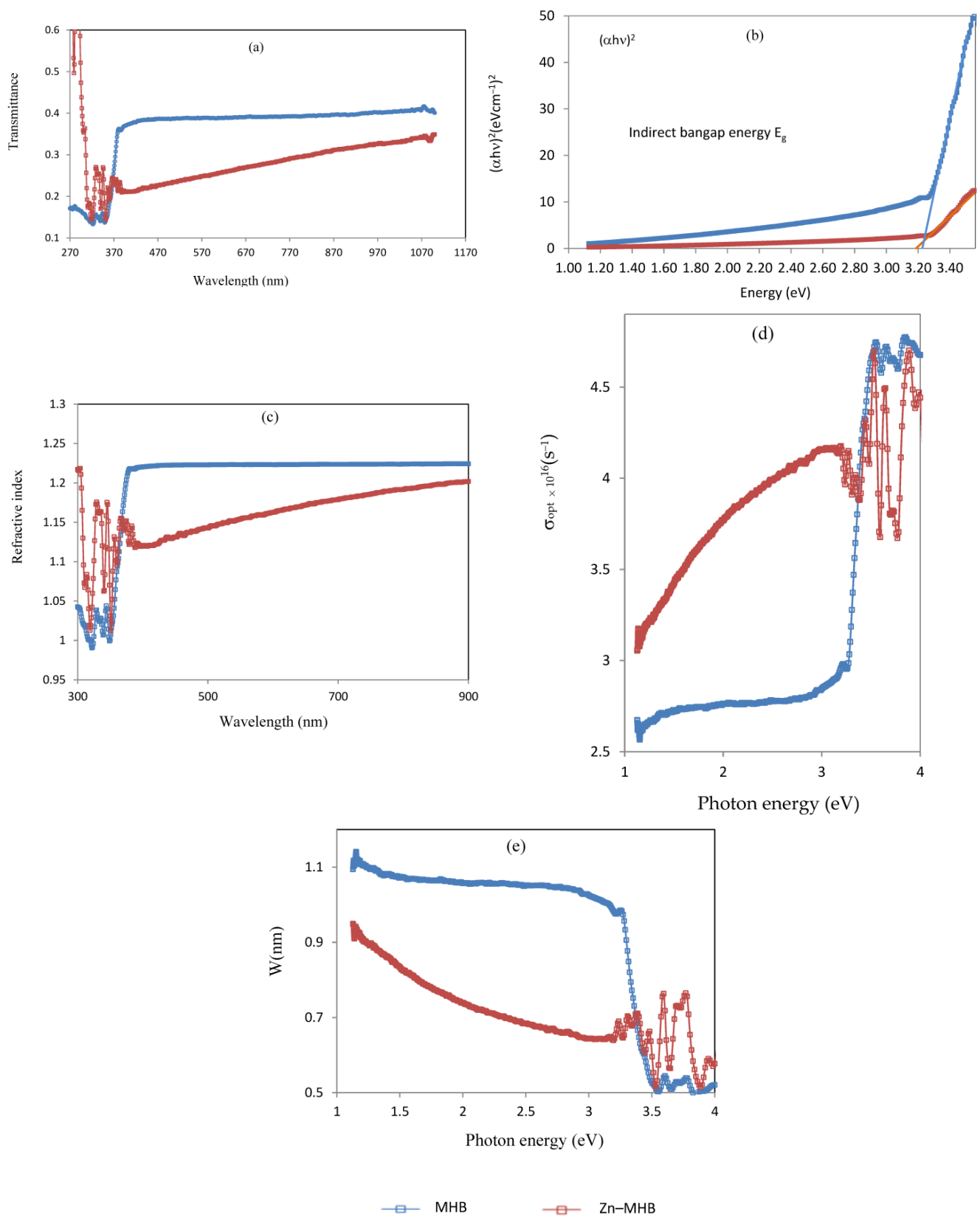


Figure 7. Variation of optical parameters for ligand and complex (a) transmittance, T; (b) band gap energy, E_g ; (c) refractive index, n ; (d) optical conductivity, σ_{opt} ; and (e) penetration depth, W . 3.1.5. Morphological Studies on the MHB and Zn-MHB.

The refractive index values (n) of the compounds may be approximately expressed by the relation [38,39]

$$n = \frac{1 + \sqrt{R}}{1 - \sqrt{R}}$$

where R is the usual reflectance in this case. The changes in n values with λ , in nm of incident light, are shown in Figure 7c. Because of certain interactions between photons and electrons, it is seen that the refractive index changes as the incident light beam's wavelength varies [40]. Additionally, this figure shows how complexation affects the refractive index of the free ligand where the chelation leads to a difference in the n values. It is evident from the data in Figure 7c that the refractive index rises gradually until it remains almost constant.

The optical conductivity (σ_{opt}) depends on the values of n and the frequency/wavelength of incident light and is given from [41]

$$\sigma_{\text{opt}} = nk\nu = nck/\lambda$$

$$K = \alpha\lambda/4\pi$$

where ν , λ , k , c , n , α and A denote the frequency, wavelength, extinction coefficient, light velocity, refractive index, absorption coefficient and absorption, respectively. Figure 7d displays the variation of σ_{opt} as a function of photon energy ($h\nu$). The diagram illustrates precisely how, for two compounds, the ligand's conductivity is nearly constant and the complex's σ_{opt} value increases with photon energy or light frequency in the range of 1–3. After this, the ligand conductivity increases in comparison to the complex, which seems to change depending on the incident light frequency.

How far light can go through a compound is determined by its penetration depth. This depth—also known as skin depth—is reached when the internal radiation intensity of the material drops to roughly 37% of its initial level. The relationship used to determine the light penetration depth (W) through the ligand and zinc complex is:

$$W = \lambda/4\pi k$$

where the wavelength and extinction coefficient are denoted by k and λ , respectively. As a result, depending on the characteristics of the material and the radiation's wavelength, electromagnetic radiation may either go away instantly or penetrate a substance very deeply. Actually, depth can provide the details with greater significance and insight. Figure 7e displays the fluctuation of W vs. photon energy. Until the photon energy is 3.3, the penetration distance of the ligand is higher than that of the complex after which the opposite happens.

Transmission electron microscopy (TEM) analysis [42] was carried out to study the morphological properties and the TEM images at the same magnification are shown in Figure 8. The TEM micrographs of both MHB and Zn–MHB exhibited regular spherical structures. While some of the Zn–MHB particles are heterogeneously dispersed and aggregated, the MHB particles appear to be mono-crystalline, non-aggregated and evenly distributed. The obtained outcome is in good agreement with the XRD findings. The nanostructure of the complex in comparison to the ligand was further verified by the TEM pictures, where MHB and Zn–MHB give average particle sizes of 116 and 95 nm, respectively. In fact, the chelation-induced change in ligand particles into zero-dimensional (0-D) nanoparticles might be regarded as a successful outcome. The nanoscale of the Zn–MHB points to the possibility of utilizing the produced Zn(II) complex in nanotechnology, in the field of medicine, environmental remediation and as quantum dots, especially in the band gap (E_g) located in the semiconductor range.

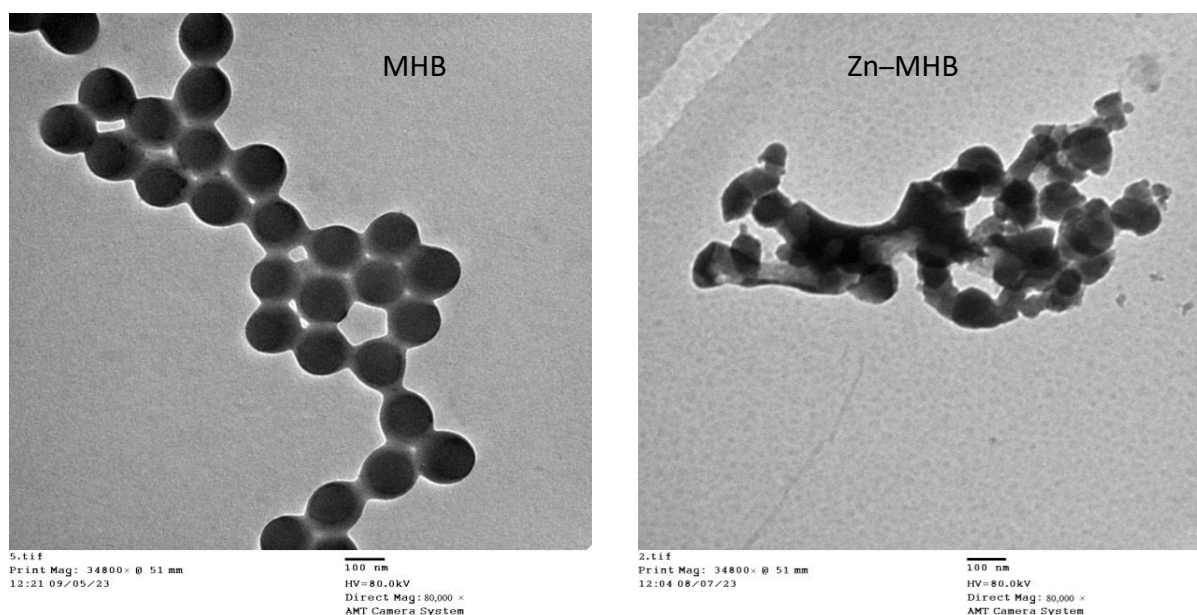


Figure 8. TEM images of MHB and Zn-MHB.

3.1.5. Antibacterial Investigation

The antimicrobial evaluation of MHB was carried out while the antimicrobial evaluation of the corresponding Zn(II) complex was not due to its insolubility, as mentioned in Section 2. The screening of the antimicrobial activity of synthesized MHB exhibits no activity against enterococcus faecalis; high activity against salmonella typhimurium; and moderate activity towards other examined bacteria (Figure 9). While the MHB did not exhibit greater activity than the reference, it exhibited beneficial activity against the tested strains of several bacteria, especially salmonella. Salmonella infections in animals used for food production are a severe public health problem since animal foods are thought to be a major source of human illness. Eggs and meat from chickens and other food animals are the most frequently found causes of infection. Salmonellosis outbreaks in humans have also been linked to milk and dairy products. Infected water may also contaminate fruits and vegetables, which could also be a source of infection. Within 24 h of infection, the *S. typhimurium*-caused salmonellosis in people and animals in food production is characterized by severe intestinal inflammation, fever and diarrhea. Because salmonella can employ a variety of virulence factors to overcome colonization resistance and cause intestinal inflammation, it is dangerous [43]. According to what was said, the increased efficacy of MHB against *Salmonella typhimurium* in comparison to gentamycin may be regarded as a distinguishing characteristic. The ability of MHB to permeate lipid membranes and block the metal binding sites in microbial enzymes serves as an example of how effective it is against bacteria [44,45]. This behavior led to the destruction of the enzymes and hence impedes the formation of proteins necessary for the further growth of the organisms [46].

3.1.6. Cytotoxic Assay

Exposure to the excess doses of chemical compounds or drugs may cause many health problems such as skin rashes, burns and kidney and lung damage, as well as impact the central nervous system, induce cancer, etc. To obtain a preliminary indication of the cytotoxicity of MHB in normal cells, MHB was evaluated against normal mammalian cell lines including those of the African Green Monkey kidney (VERO) and human normal melanocytes of skin (HFB4). The cell viability values are exhibited in Figure 10. The concentration needed to destroy 50% of the healthy cells (CC_{50}) was estimated. Human normal melanocytes had a CC_{50} of $119.45 \pm 6.31 \mu\text{g/mL}$; however, mammalian cells from the African green monkey kidney showed lesser sensitivity ($153.85 \pm 10.47 \mu\text{g/mL}$).

In general, the MHB was practically devoid of significant cytotoxic activity in normal mammalian cells [47]. Of course, this result is speculative as MHB mimics hydroxybenzoic acid to a large extent and hydroxybenzoic acid is a natural substance employed in a variety of medicinal formulations as well as food and cosmetic additives [48,49].

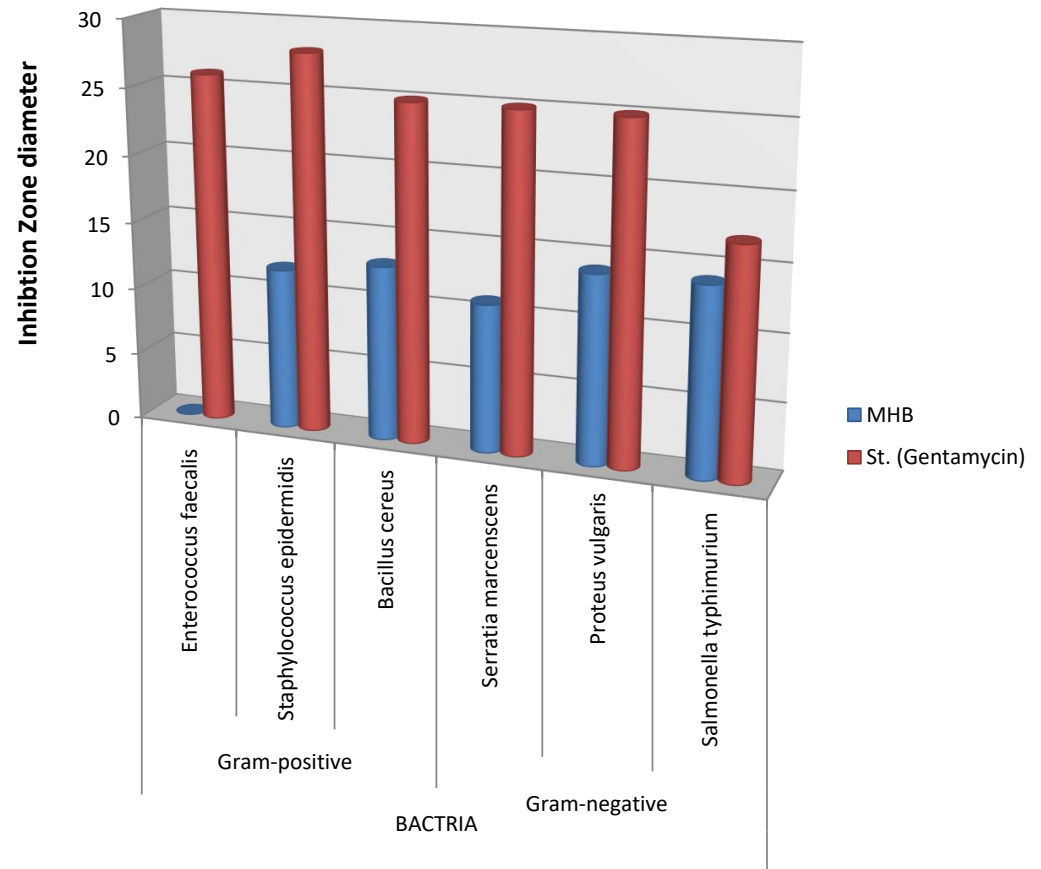


Figure 9. Antimicrobial activity for MHB.

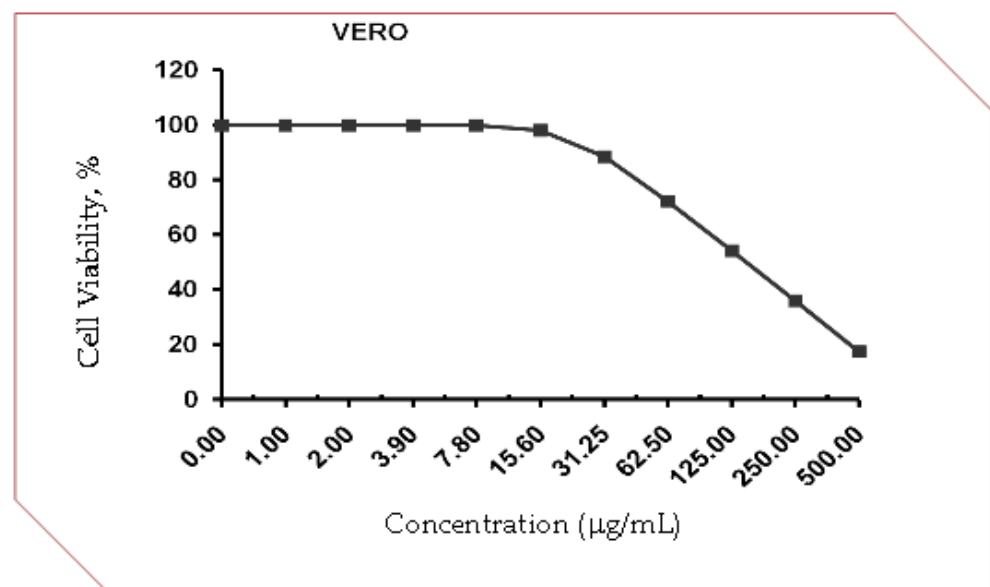


Figure 10. Cont.

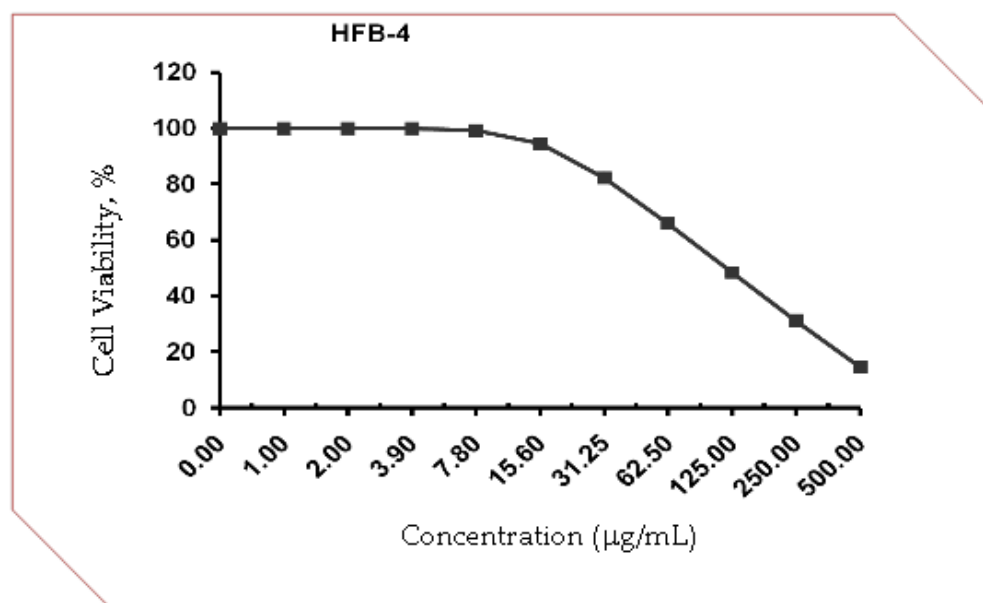


Figure 10. Evaluation of cytotoxicity against VERO and HFB-4 cell lines.

4. Conclusions

3,3'-Methylenebis(2-hydroxybenzoic acid) can be created from formaldehyde, salicylic acid and sulfuric acid. Different methods can be used to identify the MHB and associated Zn(II) complex, including elemental studies (C, H, M), FT-IR, mass, NMR and UV-Vis. Comparing theoretical and experimental elemental analysis percentages (C, H and M%) reveals that the isolated Zn(II) complex's composition matches well with the suggested formulae. The Zn(II)-3,3'-methylenebis(2-hydroxybenzoic acid) complex (Zn-MHB) displays tetrahedral conformation. The compounds' optical transmittance, band gap and optical constants were studied. As the current compounds' energy gap values fall within the range of semiconductors, they could soon be employed as raw materials for solar radiation harvesting solar cell applications. After chelation, the optical band gap and refractive index values differ. It appears that the optical conductivity and penetration depth of the compounds depend on the frequency or photon energy. The antibacterial activity of the studied MHB ligand against particular types of bacteria has been evaluated (six microorganisms). The results of this study showed that the ligand had a reasonable effect and might stop some bacteria from creating proteins, especially salmonella typhimurium. Additionally, free MHB had negligible cytotoxic effects on VERO and HFB-4, which are two types of typical mammalian cells. This was expected because the structure of the naturally occurring chemical salicylic acid is similar to that of MHB.

Author Contributions: Conceptualization, I.O.A.; methodology, A.H.A., E.S.G. and M.A.; validation, A.H.A.; formal analysis, E.S.G., O.A.H., M.A. and Y.M.A.; investigation, E.S.G. and M.A.; resources, A.H.A.; data curation, A.H.A. and M.A.; writing—original draft preparation, E.S.G. and M.A.; writing—review and editing, I.O.A., A.H.A., E.S.G., O.A.H. and M.A.; visualization, Y.M.A.; supervision, A.H.A.; project administration, I.O.A.; funding acquisition, I.O.A. All authors have read and agreed to the published version of the manuscript.

Funding: This research was funded by the Deanship of Scientific Research at Jouf University through the Fast-track Research Funding Program.

Data Availability Statement: Data are contained within the article.

Conflicts of Interest: The authors declare no conflict of interest.

References

1. Kahl, L. Ueber Condensationsproducte von Aldehyden mit Phenolen und Phenolcarbonsäuren und davon derivirende Diphenylmethanfarbstoffe. *Ber. Dtsch. Chem. Ges.* **1898**, *31*, 143–151. [[CrossRef](#)]
2. Takashi, H.; Takaaki, H.; Hyozo, S.; Alan, P.M.; Kaipenchery, A.K.; Simon, G.B.; Kata, M.M.; Tatjana, S.; Nazar, S.A.E.; Hong-Sik, H.; et al. Molecular design of lipophilic disalicylic acid compounds with varying spacers for selective lead(II) extraction. *Talanta* **2000**, *52*, 385–396.
3. Clemmensen, E.; Heitman, A.H.C. Methylene-disalicylic acid and its reaction with bromine and iodine. *J. Am. Chem. Soc.* **1911**, *33*, 733–745. [[CrossRef](#)]
4. Sivapullaiah, P.V.; Soundararajan, S. Methylene di salicylates of rare-earths. *J. Indian Inst. Sci.* **1976**, *58*, 289–293.
5. Patel, R.P.; Karampurwala, A.M.; Shah, J.R. Physicochemical studies on square planar Co^{2+} , Ni^{2+} and Cu^{2+} chelate polymers. *Macromol. Mater. Eng.* **1980**, *87*, 87–94.
6. Kaltenberg, J.; Plum, J.L.; Ober-Blobaum, J.L.; Honscheid, A.; Rink, L.; Haase, H. Zinc signals promote IL-2-dependent proliferation of T cells. *Eur. J. Immunol.* **2010**, *40*, 1496–1503. [[CrossRef](#)]
7. Kim, A.M.; Bernhardt, M.L.; Kong, B.Y.; Ahn, R.W.; Vogt, S.; Woodruff, T.K.; O'Halloran, T.V. Zinc sparks are triggered by fertilization and facilitate cell cycle resumption in mammalian eggs. *ACS Chem. Biol.* **2011**, *6*, 716–723. [[CrossRef](#)]
8. Xu, Y.; Luo, F.; Zheng, J.M. Syntheses, structures, and magnetic properties of a series of hetero-tri-, tetra- and pentanuclear $\text{Ln}^{\text{III}}\text{-Co}^{\text{II}}$ compounds. *Polymers* **2019**, *11*, 196. [[CrossRef](#)] [[PubMed](#)]
9. Chen, D.M.; Zhang, N.N.; Liu, C.S.; Jiang, Z.H.; Wang, X.D.; Du, M.A. Mixed-cluster approach for building a highly porous cobalt(II) isonicotinic acid framework: Gas sorption properties and computational analyses. *Inorg. Chem.* **2017**, *56*, 2379–2382. [[CrossRef](#)] [[PubMed](#)]
10. Li, W.D.; Guo, X.Z.; Zhang, Z.Y.; Chen, S.S. Metal(II) coordination polymers derived from mixed 4-imidazole ligands and carboxylates: Syntheses, topological structures, and properties. *Polymers* **2018**, *10*, 622. [[CrossRef](#)] [[PubMed](#)]
11. Zhang, C.H.; Chen, Y.G.; Tang, G.; Liu, S.X. Polynuclear complexes of main group and transition metals with polyaminopolycarboxylate and polyoxometalate. *Dalton Trans.* **2012**, *41*, 9971. [[CrossRef](#)]
12. Gao, F.; Chunji, N.; Ni, J. Study on mixed ligand complexes of rare earth with nitrilotriacetic acid and amino acid. *Chin. J. Appl. Chem.* **1990**, *3*, 10–13.
13. Trevin, S.; Bedioui, F.; Gomez, M.G.; Charreton, C.B. Electro polymerized nickel Micro cyclic complex—Base films design and electro-catalytic application. *J. Mater. Chem.* **1997**, *7*, 923–928. [[CrossRef](#)]
14. Ahmed, A.H.; Sherif, E.M. Methylene-disalicylic acid as a bio corrosion inhibitor for aluminum in concentrated sodium chloride solutions. *ACS Omega* **2022**, *7*, 19193–19203. [[CrossRef](#)] [[PubMed](#)]
15. Perez-Cano, H.J.; Robles-Contreras, A. Basic aspects of the mechanisms of bacterial resistance. *Rev. Med. MD* **2013**, *4*, 186–191.
16. Kantouch, A.; Atef El-Sayed, A.; Salama, M.; Abou El-Kheir, A.; Mowafi, S. Disalicylic acid and some of its derivatives as antibacterial agents for viscose fabric. *Int. J. Biol. Macromol.* **2013**, *62*, 603–607. [[CrossRef](#)]
17. Yishan, F.; Jianxin, F.; Chunjing, T.; Pengfei, L.; Bo, C. Mechanical properties and antibacterial activities of novel starch-based composite films incorporated with disalicylic acid. *Int. J. Biol. Macromol.* **2020**, *155*, 1350–1358.
18. Ghezzi, L.; Spepi, A.; Agnolucci, M.; Cristani, C.; Giovannetti, M.; Tiné, M.R.; Duce, C. Kinetics of release and antibacterial activity of disalicylic acid loaded into halloysite nanotubes. *Appl. Clay Sci.* **2018**, *160*, 88–94. [[CrossRef](#)]
19. Cushman, M.; Kanamathareddy, S. Synthesis of the covalent hydrate of the incorrectly assumed structure of aurintricarboxylic acid (ATA). *Tetrahedron* **1990**, *46*, 1491–1498. [[CrossRef](#)]
20. Thabet, M.S.; Ahmed, A.H. Ship-in-a-bottle synthesis and physicochemical studies on zeolite encapsulated Mn(II), Mn(III)-semicarbazone complexes: Application in the heterogeneous hydroxylation of benzene. *J. Porous Mater.* **2013**, *20*, 319–330. [[CrossRef](#)]
21. Mott, N.F.; Davis, E.A. *Electronic Processes in Non-Crystalline Materials*, 2nd ed.; Clarendon Press: Oxford, UK, 1979.
22. Ahmed, A.H.; Hassan, A.M.; Gumaa, H.A.; Mohamed, B.H.; Eraky, A.M. Physicochemical studies on some selected oxaloyldihydrazones and their novel palladium(II) complexes along with using oxaloyldihydrazones as corrosion resistants. *Inorg. Nano-Met. Chem.* **2017**, *47*, 1652–1663. [[CrossRef](#)]
23. Ahmed, A.H.; Hassan, A.M.; Gumaa, H.A.; Mohamed, B.H.; Eraky, A.M.; Omran, A.A. Copper(II)-oxaloyldihydrazone complexes: Physico-chemical studies; energy band gap and inhibition evaluation of free oxaloyldihydrazones toward the corrosion of copper metal in acidic medium. *Arab. J. Chem.* **2019**, *12*, 4287–4302. [[CrossRef](#)]
24. Hindler, J.A.; Howard, B.J.; Keiser, J.F. Antimicrobial agents and Susceptibility testing. In *Clinical and Pathogenic Microbiology*; Howard, B.J., Ed.; Mosby-Year Book Inc.: St. Louis, MO, USA, 1994.
25. Abo-Ashour, M.F.; Eldehna, W.M.; Nocentini, A.; Bonardi, A.; Bua, S.; Ibrahim, H.S.; Elaasser, M.M.; Kryštof, V.; Jorda, R.; Gratteri, P.; et al. 3-Hydrazinoisatin-based benzenesulfonamides as novel carbonic anhydrase inhibitors endowed with anticancer activity: Synthesis, in vitro biological evaluation and in silico insights. *Eur. J. Med. Chem.* **2019**, *184*, 111768. [[CrossRef](#)]
26. Gomha, S.M.; Riyadh, S.M.; Mahmmoud, E.A.; Elaasser, M.M. Synthesis and anticancer activities of thiazoles, 1,3-thiazines, and thiazolidine using chitosan-grafted-poly(vinylpyridine) as basic catalyst. *Heterocycles* **2015**, *91*, 1227–1243.
27. Ali, A.M.; Ahmed, A.H.; Mohamed, T.A.; Mohamed, B.H. Chelates and corrosion inhibition of newly synthesized Schiff bases derived from o-toluidine. *Transit. Met. Chem.* **2007**, *32*, 461–467. [[CrossRef](#)]

28. Pettinari, C.; Lorenzotti, A.; Pellei, M.; Santini, C. Zinc(II), cadmium(II) and mercury(II) derivatives of bis(4-halopyrazol-1-yl)alkanes: Synthesis, spectroscopic characterization and behaviour in solution. *Polyhedron* **1997**, *16*, 3435–3445. [[CrossRef](#)]
29. Adhikari, S.; Bhattacharjee, T.; Butcher, R.J.; Porchia, M.; De Franco, M.; Marzano, C.; Gandin, V.; Tisato, F. Synthesis and characterization of mixed-ligand Zn(II) and Cu(II) complexes including polyamines and dicyano-dithiolate(2-): In vitro cytotoxic activity of Cu(II) compounds. *Inorg. Chim. Acta* **2019**, *498*, 119098. [[CrossRef](#)]
30. Lal, R.A.; Basumatary, D.; Arjun, K.D.; Kumar, A. Synthesis and spectral characterization of zinc(II), copper(II), nickel(II) and manganese(II) complexes derived from bis(2-hydroxy-1-naphthaldehyde) malonyldihydrazone. *Transit. Met. Chem.* **2007**, *32*, 481–493. [[CrossRef](#)]
31. Temel, H.; Çakir, Ü.; Otludil, B.; Uğraş, H.İ. Synthesis, spectral and biological studies of Mn(II), Ni(II), Cu(II), and Zn(II) complexes with a tetradentate Schiff base ligand. complexation studies and the determination of stability constants (Ke). *Synth. React. Inorg. Met-Org Chem.* **2001**, *31*, 1323–1337. [[CrossRef](#)]
32. Joseyphus, R.S.; Nair, M.S. Synthesis, characterization and biological studies of some Co(II), Ni(II) and Cu(II) complexes derived from indole-3-carboxaldehyde and glycylglycine, as Schiff base ligand. *Arab. J. Chem.* **2010**, *3*, 195–204. [[CrossRef](#)]
33. Patterson, A. The Scherrer formula for X-ray particle size determination. *Phys. Rev.* **1939**, *56*, 978–982. [[CrossRef](#)]
34. Streetman, B.G. *Solid State Electronic Devices*, 5th ed.; Prentice Hall: Upper Saddle River, NJ, USA, 2000.
35. Karipcin, F.; Dede, B.; Caglar, Y.; Hur, D.; Ilcan, S.; Caglar, M.; Sahin, Y. A new dioxime ligand and its trinuclear copper(II) complex: Synthesis, characterization and optical properties. *Opt. Commun.* **2007**, *272*, 131–137. [[CrossRef](#)]
36. Sengupta, S.K.; Pandey, O.P.; Srivastava, B.K.; Sharma, V. Trends in Structural Mechanics: Theory, Practice. *Transit. Met. Chem.* **1998**, *23*, 349–353. [[CrossRef](#)]
37. Turan, N.; Gündüz, B.; Körkoca, H.; Adigüzel, R.; Çolak, N.; Buldurun, K. Study of structure and spectral characteristics of the zinc(II) and copper(II) complexes with 5,5-dimethyl-2-(2-(3-nitrophenyl)hydrazono)cyclohexane-1,3-dione and their effects on optical properties and the developing of the energy band gap and investigation of antibacterial activity. *J. Mex. Chem. Soc.* **2014**, *58*, 65–75.
38. Gittleman, J.I.; Sichel, E.K.; Arie, Y. Composite semiconductors: Selective absorbers of solar energy. *Sol. Energy Mater.* **1979**, *1*, 93–104. [[CrossRef](#)]
39. Belmokhtar, A.; Yahiaoui, A.; Hachemaoui, A.I.; Abdelghani, B.; Sahli, N.; Belbachir, M. A Novel Poly((2,5-diylfuran)(benzylidene)): A new synthetic approach and electronic properties. *ISRN Phys. Chem.* **2011**, *2012*, 781879.
40. Yakuphanoglu, F.; Erten, H. Refractive index dispersion and analysis of the optical constants of an ionomer thin film. *Opt. Appl.* **2005**, *4*, 969–976.
41. Paul, T.C.; Podder, J. Synthesis and characterization of Zn-incorporated TiO₂ thin films: Impact of crystallite size on X-ray line broadening and bandgap tuning. *Appl. Phys. A* **2019**, *125*, 818. [[CrossRef](#)]
42. Amin, B.H.; Ahmed, H.Y.; El Gazzar, E.M.; Badawy, M.M.M. Enhancement the mycosynthesis of selenium nanoparticles by using gamma radiation. *Dose-Response Int. J.* **2021**, *4*, 15593258211059323. [[CrossRef](#)]
43. Fabrega, A.; Vila, J. *Salmonella enterica* serovar typhimurium skills to succeed in the host: Virulence and regulation. *Clin. Microbiol. Rev.* **2013**, *26*, 308–341. [[CrossRef](#)] [[PubMed](#)]
44. Ahmed, A.H. *N,N'*-bis[2-hydroxynaphthylidene]/[2-methoxybenzylidene]amino]oxamides and their divalent manganese complexes: Isolation, spectral characterization, morphology, antibacterial and cytotoxicity against leukemia cells. *Open Chem.* **2020**, *18*, 426–437. [[CrossRef](#)]
45. Ahmed, A.H.; Hassan, A.M.; Gumaa, H.A.; Mohamed, B.H.; Eraky, A.M. Nickel(II)-oxaloyldihydrazone complexes: Characterization, indirect band gap energy and antimicrobial evaluation. *Cogent Chem.* **2016**, *2*, 1142820. [[CrossRef](#)]
46. Kavitha, P.; Reddy, K.L. Synthesis, spectral characterization, morphology, biological activity and DNA cleavage studies of metal complexes with chromone Schiff base. *Arab. J. Chem.* **2016**, *9*, 596–605. [[CrossRef](#)]
47. Mohareb1, R.M.; EL-Sharkawy, K.A.; Al Farouk, F.O. Synthesis, cytotoxicity against cancer and normal cell lines of novel hydrazide-hydrazine derivatives bearing 5H-chromen-5-one. *Med. Chem. Res.* **2019**, *28*, 885–1900.
48. Baxter, G.J.; Graham, A.B.; Lawrence, J.R.; Wiles, D.; Paterson, J.R. Salicylic acid acid in soups prepared from organically and non-organically grown vegetables. *Eur. J. Nutr.* **2001**, *40*, 289–292. [[CrossRef](#)]
49. William, P.; Coleman, M.D., III; Harold, J.; Brody, M.D. Advances in chemical peeling. *Dermatol. Clin.* **1997**, *15*, 19–26.

Disclaimer/Publisher’s Note: The statements, opinions and data contained in all publications are solely those of the individual author(s) and contributor(s) and not of MDPI and/or the editor(s). MDPI and/or the editor(s) disclaim responsibility for any injury to people or property resulting from any ideas, methods, instructions or products referred to in the content.